THE JOURNAL OF PHYSICAL CHEMISTRY B

Article

pubs.acs.org/JPCB

How Do Anions Affect Self-Assembly and Solubility of Cetylpyridinium Surfactants in Water

Wolfram Müller, Christophe Déjugnat,† Thomas Zemb, Jean-François Dufrêche, and Olivier Diat*

Institut de Chimie Séparative de Marcoule (ICSM), UMR 5257 (CEA/CNRS/UM2/ENSCM), Bagnols-sur-Cèze, France

Supporting Information

ABSTRACT: We report the specific effects of a series of anions (chloride, nitrate, and oxalate) on the solubility and self-assembly of cationic cetylpyridinium surfactants in water. The anion influence on micellization was evidenced by tensiometry and determination of Krafft temperatures. Anions strongly affect these parameters, depending on their position in the lyotropic series as well as on their "bridging" character. Scattering techniques (light, X-rays, and neutrons) were used to characterize the structures of micelles, and by solving a lateral equation of state approach, we show that chaotropic anions can be considered as adsorbed on the pyridinium head groups, inducing a decrease of the surface polarity and a Krafft temperature shift. Mixing different counteranions in various ratios led to a competition with a preferential adsorption at the micellar surface.

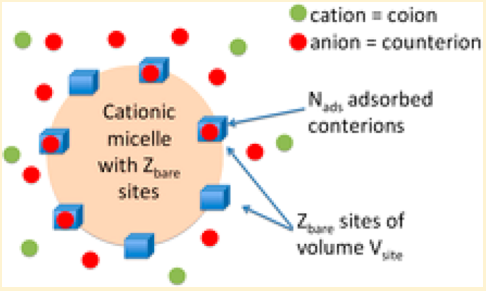

INTRODUCTION

Cationic surfactants have been widely used for a long time in a great variety of products and applications. Among them, alkylpyridinium surfactants and their derivatives are of special interest: they are used as corrosion inhibitors for steel protection,[1] in mouth rinsing formulations due to their antibacterial properties,[2] in spectroscopy as fluorescence quenchers,[3] in separation techniques like micellar enhanced ultrafiltration,[4] or as carriers through liquid membranes (pertraction).[5]

As for all the other tensides, it has been known for a long time that electrolytes have a major influence on surfactant aggregation.[6] Especially anions have a greater impact than cations, due to a higher polarizability of their valence electrons and the interplay of hydration and dispersion forces.[7] Since the pioneering work of Hofmeister who has investigated the influence of salts on the precipitation of proteins,[8] classifications of ions (so-called "lyotropic series" or "Hofmeister series") were proposed describing their ability to increase or decrease protein solubility. Such a series for anions (with H^+ as a counterion) can be listed as follows:[9,10]

$$SO_4^{2-} > HPO_4^{2-} > OH^- > F^- > HCOO^- > PO_4^{3-} > CH_3COO^- > Cl^- > Br^- > I^- > NO_3^- > ClO_4^- > SCN^-$$

Even if some ions can be exchanged along the series, Cl^- represents a borderline case: the ions on the left side of Cl^- reduce protein solubility (so-called "salting-out", "kosmotropes", or "water-structure-makers"), while the ions on the right side of Cl^- increase protein solubility (so-called "salting-in", "chaotropes", or "water-structure-breakers"). The influence of ions on colloidal interactions and on water swelling in soft matter systems along the lyotropic series has been extensively studied, and even some inversions were reported.[9,11−14] In this context, ion pairing was considered by Collins to be a critical parameter influencing micellar properties.[15] This has been confirmed quantitatively by Vlachy and co-workers.[14] It contributes to the free energy of the system, as ion pairs are less hydrated than isolated ions. Therefore, ion pairing at the water−oil interface is promoted between ions with similar free energy of hydration (kosmotropes better pair with kosmotropes, and chaotropes better pair with chaotropes).

However, ion interactions with surfactant head groups interfaces are still debated considering lateral interactions and surface entropy loss related to the 2D character of the association. Better polarizable chaotropic ions seem to have stronger dispersion interactions with interfaces than their kosmotropic counterparts.[16] Furthermore, Leontidis stated that anions could also act through direct interactions with surfaces.[11] Recently, the influence of interfacial hydration on aggregation parameters has been discussed, and "interfacial" water (in contrast to the "bulk" water) is considered as an integral part of the aggregate. Therefore, the aggregate structure is sensitive to the balance of short-range interactions within the interfacial region and the hydration of the head groups and the counterions. For example, sphere-to-rod transitions can occur when dehydration of the interfacial region favors the formation of head group−counterion pairs, as evidenced from chemical trapping experiments.[17,18] Recently, the surfactant head groups themselves have been considered as chaotropic or kosmotropic moieties and were classified in a Hofmeister series in order to

Received: September 20, 2012
Revised: December 11, 2012
Published: January 10, 2013

   dx.doi.org/10.1021/jp3093622 | J. Phys. Chem. B 2013, 117, 1345−1356

explain and predict their interaction with a given type of counterion.[14,19] However, many studies of specific ion effects on surfactant aggregation have been realized using mixtures of counterions: those coming from the surfactants and the other provided by the bulk electrolytes, leading to much more complex situations.[20−22]

In the present paper, we have studied the influence of anions on cetylpyridinium (CP) self-organization in the presence of electrolytes. We took care of using the same counterions for CP and the electrolytes, and no additional cation was introduced thanks to the use of acids as electrolytes. CP surfactants have been investigated in the past, but we think that a proper and extensive reinvestigation using all kinds of scattering and other methods should be interesting and useful. To conduct this study properly, we have considered three CP salts involving single anions at very different positions in the lyotropic series: chloride (borderline), nitrate (chaotropic), and oxalate (kosmotropic). This latter might be surprising, as acetate would have been a more obvious choice, but we could not obtain satisfying results with this anion. In fact, the choice of oxalate proved to be quite interesting, leading to some contrasting results with the simpler counterions.

In the first part, we show how micellization parameters and Krafft temperatures of CP surfactants vary as a function of the kind of anion and on the ionic strength. The aim of this study was to point out different interactions occurring between CP head groups and anions. The second part of this paper focuses on an extensive structural analysis of the aggregates formed by CP derivatives by means of scattering experiments (light, neutrons, and X-rays). These complementary techniques were conducted to access the sizes and the shapes of the aggregates, as well as aggregation numbers and especially surface areas per head group. Indeed, this latter parameter gives significant information on the way CP head groups and anions interact (adsorption, condensation, binding, etc.). At this point, a competition experiment was realized between chloride and nitrate to determine the preferential interaction with the CP interface. Finally, in the third part, a theoretical model based on a lateral equation of state is build up taking into account different contributions to the free energy of the system. This model also gives access to the surface area per head group, in accordance with experimental results. Moreover, it was used to determine which contributions were preferentially involved in the specific interactions between CP and the selected anions.

EXPERIMENTAL SECTION

Materials. Absolute ethanol, aqueous hydrochloric acid (37%), aqueous nitric acid (65%), and oxalic acid (puriss. p.a.) were reagent-grade products purchased from Sigma Aldrich and used as received. Cetylpyridinium chloride (CPC, 99% purity, ACS reagent-grade) was also purchased from Sigma-Aldrich and recrystallized twice in absolute ethanol. Cetylpyridinium nitrate (CPN) and cetylpyridinium oxalate (CP_2Ox) were prepared by repeated recrystallizations (six times) of purchased CPC in 3 M aqueous nitric acid or 1 M aqueous oxalic acid, respectively, and further purified by five recrystallizations in Milli-Q water. The products were then dried under a vacuum. All three surfactants were of matt white color and possessed finely dispersed texture. Infrared spectroscopy and elementary analysis of the surfactants confirmed the purity and the absence of hydration water (Supporting Information, section 1). Water used in all experiments was produced by a two-stage Milli-Q system from Millipore and had a resistivity higher than 18.2 MΩ·cm.

Sample Preparations and Krafft Temperature Determination. All samples were prepared by weighting accurately the dry surfactants into presealed polypropylene tubes before adding the corresponding aqueous acid solutions, which were filtered through 100 nm polytetrafluoroethylene (PTFE) filter units (Millipore) before use. Thus, impurities like dust residues which represent a major source of error for light scattering measurements were reduced to a minimum. Stock solutions containing 30 mM of each cetylpyridinium salt were diluted with the corresponding acid solutions to obtain the targeted surfactant concentration. All dilution steps were carried out above the Krafft temperatures to ensure complete solubility of the surfactants. The Krafft temperatures were measured by gradually heating the samples in a thermostatic Julabo MB-5 M bath beginning from 4 °C up to complete dissolution of CP crystals, which was observed visually. The heating steps were 0.5 °C with 10 min equilibration time at each temperature.

Surface Tension. Surface tension measurements were carried out with a Krüss DSA 100 tensiometer by recording with a CCD camera the shape of a solution droplet in air. Hamilton 1750 TLL syringes (500 μL) were used with Krüss steel needles of known diameter (1.494−2.090 mm). The samples of CPC and CPN were equilibrated 1 day at 25 °C and those containing CP_2Ox at 55 °C for 3 h before the measurements. Each surface tension isotherm was averaged over three to six experiments. Due to the high Krafft point of CP_2Ox (about 55 °C), the surface tension measurements were carried out in an environmental chamber with temperature (TC-40) and humidity (HC-10) controls. Droplet evaporation was reduced significantly by placing a small vessel filled with water.

Static and Dynamic Light Scattering Measurements (SLS and DLS). They were carried out using a Malvern ZEN3600 Zetasizer Nano ZS apparatus operating at fixed angle (173°, backscatterer). The wavelength of the 4 mW He−Ne laser was 633 nm. The device allows conducting DLS and SLS measurements one after another while keeping the sample at the same position. The detectable particle sizes ranged from 0.6 nm to 6 μm and the molecular weight from 10^3 to 10^7 Da. Prior to each measurement, the samples were heated in a thermostatic bath for 15 min at 35 °C (CPC, CPN) or 60 °C (CP_2Ox), before 60 μL of solution was transferred into a 45 μL quartz cell (Hellma) and sealed with a Teflon cap. All measurements were carried out at these two temperatures for CPC, CPN, and CP_2Ox, respectively, to prevent the surfactant from precipitation. In order to improve the statistics of the measurement, each point was measured twice. The primary data analysis was done by the *DTS (Nano)* software (V. 5.10) furnished with the apparatus. The Smoluchowski algorithm was used to extrapolate the diffusion coefficient of the aggregates and determine the intensity-weighted size distribution. Measurements were carried out with regard to solvent viscosity. The measurement procedure for static light scattering experiments started with the dark count of the beam intensity followed by the analysis of the pure solvent. For the scattering, standard toluene was taken with a Rayleigh ratio of 1.35×10^{-5} cm^{-1} and a refractive index of 1.496 at 35 °C. The differential refractive index increment dn/dc was taken from Anacker and had a value of 0.138 $mL \cdot mg^{-1}$ for CPN and 0.161 $mL \cdot mg^{-1}$ for CPC.[23,24]

Small-Angle X-ray and Neutron Scattering Measurements (SAXS and SANS). SAXS measurements were realized at the ESRF facility in Grenoble (France) at the D2AM beamline. The X-ray energy was mainly fixed at 13 keV, resulting in a wavelength of 0.95 Å. A FOC Princeton 1152*1242 CCD

detector was positioned at 72 cm; hence, the covered q-range was from 1.5×10^{-2} Å to 4×10^{-1} Å^{-1}. The samples were transferred into glass capillaries of known thickness (between 1.5 and 2.5 mm) and measured at fixed temperature (controlled within 0.1 °C). The beam size at the sample holder was 1 mm^2. The observed intensities were corrected for transmission, solvent, and detector response. SANS experiments were carried out at the LLB facility in Saclay (France) at the PAXE spectrometer. All samples were prepared in deuterated solvents obtained from D_2O, concentrated DCl, and concentrated DNO_3. Deuterated oxalic acid was obtained by dissolving oxalic acid in D_2O. Surfactant concentrations ranged from 5 to 100 mM. The samples were placed into quartz cells. The neutron wavelengths were 6 and 4 Å. The covered q-range from 0.01 to 0.6 Å^{-1} was obtained by adjusting two detector positions, at 5 and 1 m. The 2D isotropic scattering patterns were azimuthally averaged, and standard corrections were applied to convert scattered intensities in absolute scale.

RESULTS AND DISCUSSION

Micellization Parameters and Krafft Temperatures. Critical micellar concentrations (cmc's) of the three surfactant systems in water were determined by surface tension measurements as a function of surfactant concentrations. The experiments were realized at 20 °C for CPC and CPN and at 55 °C for CP_2Ox to ensure surfactant solubility. Surface tension isotherms showed classical profiles (Supporting Information, section 2). From these curves, cmc, surface tensions at cmc (γ_{cmc}), and Gibbs molecular interfacial areas (a_G) were determined and are reported in Table 1.

Table 1. Micellization Parameters of CPC, CPN, and CP_2Ox in Water: Critical Micelle Concentrations (cmc's), Surface Tensions at cmc (γ_{cmc}), and Gibbs Molecular Interfacial Areas (a_G)

surfactant	cmc (mM)	γ_{cmc} (mN·m^{-1})	a_G (nm^2)
CPC	0.9 ± 0.2	43.6 ± 0.4	0.66 ± 0.2
CPN	0.5 ± 0.1	37.7 ± 0.4	0.43 ± 0.2
CP_2Ox	0.1 ± 0.02	38.1 ± 0.4	0.51 ± 0.2

The cmc values observed for CPC and CPN are in good agreement with literature data.[20,25−29] Moreover, the Gibbs molecular interfacial area per surfactant head group appears slightly smaller for CPN compared to CPC. This effect can be associated to a larger screening of the micellar surface charges in the case of CPN, reducing therefore electrostatic repulsions between head groups. With nitrate ions being considered as chaotropes,[14] this could be due to slightly larger dispersion interactions between nitrate anions and pyridinium head groups.

In the case of CP_2Ox, a lower cmc value of 0.1 mM was found. Micellization is promoted compared to CPN and CPC because we can suppose that repulsive electrostatic interactions between head groups are more effectively reduced. This can be explained by considering a strong interaction of the pyridinium groups by the divalent oxalate anion as a bridging effect. This is supported by the infrared spectrum of CP_2Ox, where the oxalate anion remains fully deprotonated (Supporting Information, section 1). Then, a somehow stronger anion−surfactant head group pairing for nitrate and oxalate generates lower electrostatic repulsions, with a closer "lateral" distance between surfactants at the water/air interface, according to the Ninham−Mitchell model of ionic micelle self-assembly.[30]

Krafft temperatures (T_K) were determined in order to get information about the solubilities of the systems, depending on the type of anion and on the ionic strength. Besides nitrate and chloride, acetate had been first envisaged as a more kosmotropic monovalent anion. However, in this case, only samples in 3 M acetic acid showed T_K slightly above freezing (5 °C), whereas determination of solubility temperature was not possible at lower acetate concentrations because all samples remained soluble down to 0 °C. For this reason, it was not possible to prepare and purify CPAc. Other monovalent carboxylates with hydrocarbon chains longer than C_2 could act as cosurfactants for cetylpyridinium, and they were therefore not good alternatives. Instead, the divalent oxalate anion has then been considered.

In all cases, surfactant concentrations were 10 mM (well above the cmc). For each considered anion, the corresponding acid (HCl, HNO_3, or oxalic acid H_2Ox) was used as bulk electrolyte to tune the ionic strength. Acid concentrations varied from 0 to 1 M, and the results are reported in Figure 1.

In the case of monovalent anions, T_K have first been determined in water with T_K = 18 °C for CPC and T_K = 17 °C

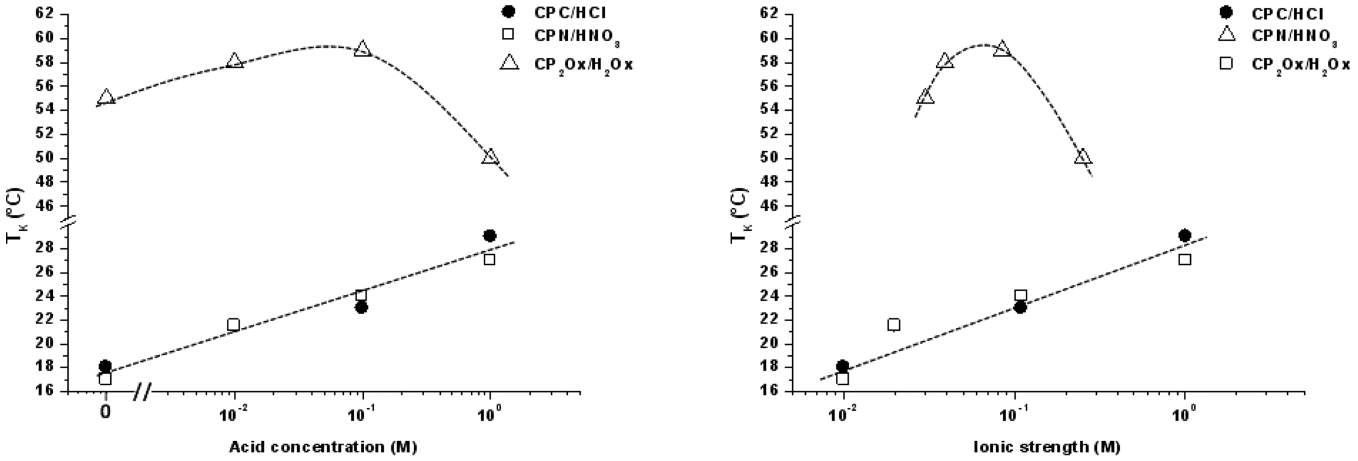

Figure 1. Variation of Krafft temperature (T_K) as a function of bulk acid concentration (left) or ionic strength (right), for aqueous 10 mM cetylpyridinium surfactants with chloride (filled circles), nitrate (open squares), and oxalate (open triangles) as counteranions. Dashed lines are drawn as eye guides.

dx.doi.org/10.1021/jp3093622 | J. Phys. Chem. B 2013, 117, 1345−1356

for CPN. We should point out that T_K values reported in the literature for CP surfactants strongly depend on experimental conditions. For example, the T_K of CPN in pure water was measured to be 11 °C by Heckmann and Abezgauz,[20,26] whereas a value of 17 °C was found by Perche[27] and us. This could be related to the observations of Sasaki who has reported that CPC forms a metastable state during the Krafft transition with its stability depending on the cooldown kinetics resulting in long conversion times to the crystalline state.[31,32] Thus, differences in taking into account incubation times are more likely to be the reason for the slight differences observed. Upon increasing ionic strength, T_K of CPC and CPN increased up to 10 °C above the values obtained in pure water which is in agreement with data reported by Nakayama.[33] On one hand, this can be explained again by the screening of repulsive electrostatic interactions between polar head groups upon addition of electrolytes. This induces a closer packing of the surfactants and favors stronger hydrophobic interactions between aliphatic chains. On the other hand, chaotropic counterions compete with charged head groups for hydration water. Both mechanisms lead to a reduced surfactant's solubility and to higher T_K values. In our case, no significant difference between chloride and nitrate on T_K values could be evidenced. However, Heckmann and Perche observed an increased T_K of CP while increasing anion polarizability in the halide series (Cl^-, Br^-, and I^-)[26,27] and more polarizable ions should interact with interfaces through stronger dispersion forces.[16] With the nitrate anion being positioned between chloride and bromide or beyond the iodide in the lyotropic series (depending on the cation), we expected therefore to observe some differences in T_K values. Apparently, this polarizability effect between chloride and nitrate in interaction with a positive pyridinium group was too weak in our systems to be clearly evidenced.

In the case of divalent oxalate anion, T_K was found to be 55 °C in pure water which is much higher than in the case of monovalent anions. Morover, upon increasing oxalic acid concentration, T_K values remained about 30 °C higher than for monovalent anions, except for the sample in 1 M oxalic acid where T_K drops even below the reference point of CP_2Ox in pure water. The globally higher T_K values observed with oxalate can be explained as mentioned previously by a bridging interaction of two pyridinium head groups by one oxalate anion (Ox^{2-}), yielding to a less flexible and less soluble surfactant assembly. On the other hand, the peculiar drop in T_K observed for CP_2Ox in 1 M H_2Ox (T_K = 50 °C) might be related to the acid speciation which varies as a function of the pH (Supporting Information, section 3). Indeed, upon increasing oxalic acid concentration, monovalent species (HOx^-) and undissociated acid (H_2Ox) are favored and ionic strength is not trivially related to acid concentration. Therefore, the bridging effect of Ox^{2-} becomes less important at high oxalic acid concentration, inducing a decrease of T_K. However, this bridging effect seems to be the major effect, overlapping the screening of charges tuned by the ionic strength.

Structural Analysis: Scattering Experiments. In this section, we show the results obtained from scattering experiments (light, neutrons, and X-rays) conducted on CP surfactant solutions. These techniques afforded information related to the size, shape, and aggregation numbers of the aggregates formed. Moreover, they are complementary because they probe the interfaces between water and aggregates at various depths. The main aim of this extensive characterization was to access the surface areas per head group which are linked to the way CP interacts with anions.

Dynamic and Static Light Scattering (DLS and SLS). DLS was first used to get preliminary information about the size of the aggregates, by measuring their hydrodynamic radius r_L. Sample series with varying CP concentrations from 0.1 to 30 mM were prepared in acid solutions at concentrations ranging from 0.01 to 3 M. Above the cmc, aggregates were clearly observed and illustrative intensity-weighted size distributions are shown in Figure 2 in the case of 10 mM CP in 1 M acids (all measurements are reported in Supporting Information, section 4).

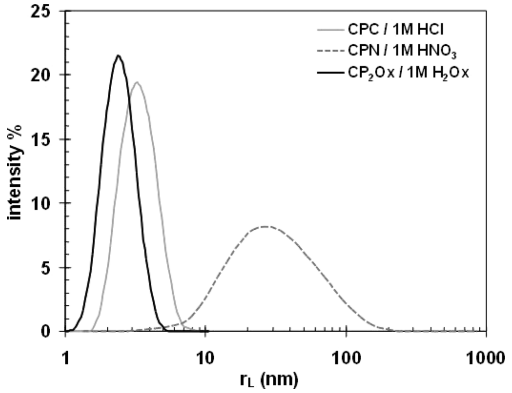

Figure 2. Intensity-weighted size distributions for CP aggregates (10 mM) in 1 M HCl, HNO_3, and H_2Ox (high ionic strength), respectively, as determined by DLS.

Size distributions of CPC and CP_2Ox aggregates in 1 M acid were rather narrow with r_L = 3−4 nm, while a broader size distribution of much larger aggregates was found for CPN aggregates. These size distributions of CP aggregates have been observed also by Anacker[24] and Abezgauz[20] and were attributed to the existence of spherical micelles for CPC and cylindrical micelles for CPN.

When decreasing acid concentrations, no significant differences were observed in the case of CPC and CP_2Ox with still the presence of small micelles (r_L = 3−4 nm). Only signals from CPN aggregates showed dependence to the nitric acid concentration: below 0.1 M HNO_3, narrow size distributions were observed similar to CPC and CP_2Ox. This is attributed for CPN to a transition from spherical to cylindrical micelles, which occurred between 0.01 and 0.1 M HNO_3. This phase transition was observed by many authors in similar cases, and the phenomenon was explained by a reduction of the surface area per surfactant head group due to the adsorption of nitrate ions on the micellar interface. Thus, repulsive head group interactions are reduced enough, leading to an elongation of the micelles toward cylindrical geometry (with a packing parameter increasing from a value below 1/3 up to a value of 1/2). As this phenomenon did not occur with CPC, even in 3 M HCl, we postulate that the charge screening effect due to ionic strength is not strong enough to induce phase transition; At that stage, we can suppose that at the opposite of nitrate ions and whatever the ionic strength chloride anions do not adsorb on the micellar interface. This is more or less consistent with the more chaotropic property of nitrate compared to chloride ions, the former being much more in competition with the hydration water molecules. The case of CP_2Ox is more specific with a strong interaction through a supposed bridging effect but without an adsorption onto the micellar surface because oxalate anions remain highly hydrated.

dx.doi.org/10.1021/jp3093622 | J. Phys. Chem. B 2013, 117, 1345−1356

Whatever the ionic strength, the CP_2Ox micelles remain spherical and small.

SLS measurements were also conducted on the same samples in order to get an estimation of the molecular weight of the aggregates by using the Debye-plot analysis.[34] According to the known relation $N_{agg} = M_W/M_0$, where M_0 stands for the molecular mass of one CP molecule plus counterion, we could determine the aggregation number N_{agg} for samples consisting of spherical micelles. Furthermore, from the aggregation number and the hydrodynamic radius, we could calculate the surface area per head group a_L of one monomer in the micelle using the equation $a_L = (4\pi r_L^2)/N_{agg}$ (all results are reported in Supporting Information, section 4). In contrast to the sterical surface area per head group ($a_0 = 0.36$ nm^2 for CP), the parameter a_L takes into account the interactions between the head groups and counterions. a_L corresponds thus to the equilibrium surface area per head group determined for a defined set of conditions (ionic strength, surfactant concentration, etc.) by light scattering. Although this approach should be considered with great care (SLS measurements were conducted at only one angle), satisfying results were obtained for CPC in HCl. The N_{agg} value was found to be about 105, corresponding to a a_L value of about 1.2 nm^2. In the case of CPN, the signal quality at low acid concentration was not satisfying enough for accurate interpretation. For CP_2Ox micelles, the surface areas per head group were very high, with values ranging from 1.2 up to 6 nm^2. Intermicellar interactions are likely to account for the low M_W measured, resulting in low N_{agg} and overestimated a_L. Therefore, we did not go further with this preliminary investigation by SLS.

Small Angle Neutron Scattering (SANS). SANS experiments have been carried out to refine information on CP aggregation. All measurements have been realized using hydrogenated surfactants in fully deuterated solvents. Assuming that interactions between aggregates are negligible in the case of sufficiently diluted solutions, the scattered intensity $I(Q)$ can be expressed as follows:[35]

$$I(Q) = \Phi \cdot V_{objects} \cdot (\Delta\rho)^2 \cdot P(Q) \quad (1)$$

In this equation, Q is the scattering vector ($4\pi/\lambda \sin(\theta/2)$ with θ the scattering angle), Φ denotes the volume fraction of the scatterers, $V_{objects}$ represents their volume, and $\Delta\rho$ is their difference in scattering length density (SLD) compared to the solvent. $P(Q)$ is the form factor of the objects, and analytical expressions have been reported for various geometries.[36] SANS profiles have been measured for 5 mM CPC, CPN, and CP_2Ox at various acid concentrations (namely, 0−1 M solutions of DCl, DNO_3, and D_2Ox in D_2O), and they are reported in the Supporting Information, section 5. In Figure 3 are presented selected scattering profiles and the corresponding modeling adjustments taking into account a Gaussian distribution of micelle radius.

For CPC in DCl and CP_2Ox in D_2Ox, the profiles have been successfully adjusted only at high ionic strength (with 0.1 M DCl and 1 M D_2Ox, respectively) with eq 1 in absolute scale, using a form factor for homogeneous spherical aggregates with a minimum of structural parameters. Indeed, at lower ionic strength, an interaction peak due to electrostatic repulsion is visible at low Q-values (see Supporting Information, section 5) and could be taken into consideration in a more complex analysis. However, the overlapping of the scattering curves at larger Q, whatever the ionic strength, suggests a similar specific surface for the CP self-assembly and therfore a global micellar

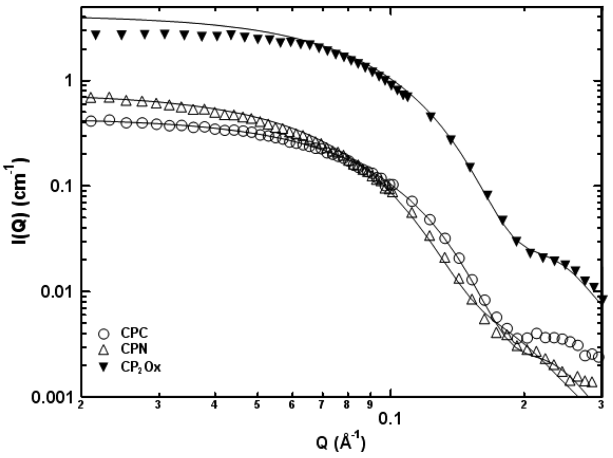

Figure 3. Selected SANS profiles of non-interacting spherical micelles formed by CPC (5 mM in 0.1 M DCl, open circles), CPN (5 mM in 0.03 M DNO_3, open triangles), and CP_2Ox (49 mM in 1 M D_2Ox, filled triangles). Solid lines are adjustments of the curves using the homogeneous sphere model.

structure that does not vary for CPC and CP_2Ox. On the other hand, for CPN in DNO_3, this model is only valid up to 0.03 M acid concentration. Beyond 0.03 M, the scattered intensity for CPN increases at low Q values (see spectrum B in Supporting Information, section 5), a clear indication for the appearance of larger aggregates. All of these indications support that spherical micelles were formed by cetylpyridinium surfactants under these conditions, and the structural parameters are described in the following paragraph.

As a first approximation, the $\Delta\rho$ value was considered the same for all series. It was computed by taking the difference between the SLD value of hexadecane (-0.43×10^{10} cm/cm^3) to represent the core of the micelles and D_2O ($+6.37 \times 10^{10}$ cm/cm^3) to represent the solvents and hydrated head groups. Indeed, with the resolution of our experiment, we were not able to consider a shell with the hydrated pyridinium heads with a different contrast. Nevertheless, from the fitting curves, micellar volumes were determined, from which structural parameters of spherical micelles could be extracted. Indeed, the following equations afforded the structural radius r_N, the aggregation number N_{agg} ($V_{mol} = 0.54$ nm^3 being the molecular volume of CP calculated from Fedors' tables[37]), and the head group surface area a_N "seen" by the neutrons:

$$r_N = (3 \cdot V_{objects}/4\pi)^{1/3} \quad (2)$$

$$N_{agg} = V_{objects}/V_{mol} \quad (3)$$

$$a_N = 4\pi \cdot r_N^2/N_{agg} \quad (4)$$

Results are reported in Table 2.

Structural radii appeared to be slightly different, with the larger one for CPN and the smallest one for CP_2Ox micelles, suggesting that counterions for CPC and CP_2Ox did not influence significantly the aggregation behavior of the surfactant as well as for CPN below a given ionic strength. However, while intermicellar interactions were screened out completely in the case of CPC in 0.1 M DCl, some weak interactions were still remaining in the case of CP_2Ox in 1 M D_2Ox. This shows that, first, what we consider as a bridging effect is not so efficient as a charge screening effect and, second, does not induce a strong reduction of area per molecule (whatever the speciation of oxalic

dx.doi.org/10.1021/jp3093622 | J. Phys. Chem. B 2013, 117, 1345−1356

Table 2. List of Parameters Used to Adjust SANS Profiles of the CPC, CPN, and CP2Ox Scattering Curves in the Case of Lowest Interactions between Aggregates, and the Resulting Structural Parameters of Spherical Micelles

solvent	Φ_v-CMC	$\Delta\rho$ (cm/cm^3)	$V_{objects}$ (nm^3)	r_N (nm)	N_{agg}	a_N (nm^2)
0.1 M DCl	0.0014	6.80×10^{10}	82.4 ± 25	2.7 ± 0.25	151 ± 45	0.6 ± 0.12
0.03 M DNO_3	0.0015	6.80×10^{10}	102.1 ± 31	2.90 ± 0.25	189 ± 50	0.56 ± 0.08
1 M D_2Ox	0.0159	6.80×10^{10}	54.3 ± 15	2.35 ± 0.17	100 ± 27	0.7 ± 0.1

Table 3. List of Parameters Used to Adjust SAXS Profiles of the CPC and CPN Scattering Curves, and the Resulting Structural Micellar Parameters (Solvent SLD = 0.331 e$^-$/nm^3)

solvent	r_{core} (nm)	r_{shell} (nm)	r_X (nm)	core SLD	shell SLD (e$^-$/Å^3)	N_{agg}	a_X (nm^2)
D_2O	2.0 ± 0.01	0.5 ± 0.01	2.5	0.26 ± 0.002	0.369 ± 0.002	121	0.65
0.01 M DCl	2.0	0.49	2.49	0.26	0.367	119	0.65
0.1 M DCl	2.0	0.49	2.49	0.255	0.365	119	0.65
1 M DCl	1.9	0.47	2.37	0.255	0.362	103	0.68
D_2O	2.0 ± 0.01	0.53 ± 0.01	2.53	0.253 ± 0.002	0.367 ± 0.002	125	0.64
0.01 M DNO_3	1.9	0.63	2.53	0.26	0.353	125	0.64
0.1 M DNO_3	1.7	0.63	2.33	0.282	0.362		
1 M DNO_3	1.7	0.63	2.33	0.282	0.353		

acid in the solution, divalent, monovalent, or neutral forms), and hence sphere-to-rod transitions like for nitrate: this is also a direct proof of the large volume brought in by oxalate in either Stern or Palisade layers.

Finally, no changes in radii were observed upon increasing acid concentration, as was also analyzed from static and dynamic light scattering data analysis (see Supporting Information, section 4). Regarding aggregation numbers, the values found were slightly superior to the value reported by Anacker (N_{agg} = 117, 15 mM CPC in 0.06 M NaCl),[23] but surface per surfactant ionic heads deduced from the spectra adjustments are comparable with those obtained from surface tension measurements. In the case of CPN, spherical micelles presented a larger structural radius and aggregation number, and slightly smaller surface area per head group than what was observed for chloride and oxalate (even if the error bars are quite large!). This might be again attributed to the tendency of nitrate to better interact with micelle interfaces than chloride or oxalate, inducing a more effective screening of electrostatic repulsions between pyridiniums. Hence, a_N = 0.56 nm^2 and this value tends to the theoretical value for cylindrical geometry (a_N < 0.5 nm^2), suggesting that the sample in 0.03 M DNO_3 was close to the sphere-to-rod transition. Indeed, the scattered intensity for CPN in 0.1 M DNO_3 increased at low Q values (see spectrum B in Supporting Information, section 5), and the Q^{-1} power law of $I(Q)$ is a clear indication for the appearance of cylindrical micelles. Therefore, the sphere-to-rod transition takes place between 0.03 and 0.1 M bulk nitrate. For similar concentrations of CPC (10 mM) in 0.15 M $NaNO_3$, Abezgauz has also observed long thread-like micelles by cryo-TEM experiments,[20] confirming our interpretation based on neutron scattering. As it was not possible to detect the lower limit of this Q^{-1} region in the SANS profile, the length of cylindrical micelles formed by CPN in 0.1 M DNO_3 could not be estimated. In this context, Odjik stated that the total length of cylindrical micelles strongly depends on the surfactant concentration and on the ionic strength.[38]

Small Angle X-ray Scattering (SAXS). Combined SAXS/SANS studies allow one to probe eventual condensation of counterions onto micelles, as this effect is expected to impact the scattering signature.[39,40] Equation 1 applies also for SAXS; only the numerical value of the contrast in scattering length density of $\Delta\rho_e$ changes, and it is now related to the difference of the electron scattering length density between the sample and the solvent. The calculation of ρ_e for a given compound can be found elsewhere.[17] Measurements have been carried out on CPC and CPN series, using the same samples that were previously analyzed by SANS: the surfactant concentration was 5 mM, and acid concentrations ranged from 0 up to 1 M. Scattering profiles of both series can be found in Supporting Information, section 6.

Regarding CPC series, the signature of the scattering curves suggested a spherical morphology for the aggregates. It came from the round-shaped decline of $I(Q)$ at medium Q values and from the first oscillation of the form factor at high Q values, indicating additionally a relatively monodisperse distribution of aggregates. Effectively, data were efficiently adjusted using a spherical core−shell model with different ρ_e for the micellar core, the micellar shell, and the solvent (X-rays are much more sensitive to the shell electronic contrast). The same contrast parameters were used from 0 up to 0.1 M DCl, by using a radius of 2.0 nm for the hydrocarbon core and a 0.22 nm thick shell. The latter was increased to 0.23 nm for 1 M DCl.

Similarly to SANS, adjustments of SAXS profiles were obtained using the above-mentioned parameters and spherical core−shell model. They afforded structural parameters (as seen from X-rays) using the following equations (V_{mol} = 0.54 nm^3 and V_{chain} = 0.45 nm^3 was the volume of the C_{16} chain calculated from Fedors' tables,[37] a value which was also used by Heindl[41]):

$$r_X = r_{core} + r_{shell} \quad (5)$$

$$N_{agg} = (4\pi \cdot {r_{core}}^3)/(3 \cdot V_{chain}) = (4\pi \cdot {r_X}^3)/(3 \cdot V_{mol}) \quad (6)$$

$$a_X = (4\pi \cdot {r_X}^2)/N_{agg} = (3 \cdot V_{mol})/r_X \quad (7)$$

Results are reported in Table 3. Although such adjustments were a simplification of the real state (counterion screening, interactions between head groups, and hydration were not considered), the results concerning a_X were close to the values obtained by SANS analysis. A shell thickness between 0.47 and 0.63 nm used in the treatment is of the order of the Heindl results,[41] while Stigter and Abezgauz reported a smaller size of the pyridinium head group (0.28[42] and 0.276 nm,[20] respectively). In the case of CPN surfactants, results were also comparable to SANS. The scattering curves of CPN in D_2O or in 0.01 M DNO_3 showed typical signatures of spherical aggregates at first

dx.doi.org/10.1021/jp3093622 | J. Phys. Chem. B 2013, 117, 1345−1356

approximation, and they were adjusted like in the case of CPC. For samples at higher nitrate concentrations, we observed an increase of $I(Q)$ intensities at low Q values. This was consistent with results from SANS, and it was again attributed to a sphere-to-rod transition. Therefore, SAXS profiles corresponding to samples in 0.1 M DNO_3 and 1 M DNO_3 were analyzed considering a cylindrical core−shell model for the form factor $P(Q)$.[36] In such a model, the aggregation number and surface area per head group are expressed as follows (l_{cyl} denoting the cylinder length):

$$N_{agg} = (\pi \cdot r_{core}{}^2 \cdot l_{cyl})/V_{chain} = (\pi \cdot r_X{}^2 \cdot l_{cyl})/V_{mol} \quad (8)$$

$$a_X = (2\pi \cdot r_X \cdot l_{cyl})/N_{agg} = (2 \cdot V_{mol})/r_X \quad (9)$$

As the lengths of cylindrical micelles l_{cyl} were not determined, N_{agg} could not be calculated, contrary to a_X values that depended only on r_X, and which are reported in Table 3.

For CPN series, the shell SLD was close to values used for CPC series (except when spherical micelles are transformed into cylinders for which the density is close to those of C16 alkane), although shell thickness was slightly higher for nitrate samples than for chloride ones. This might be attributed to partial adsorption of nitrate ions onto the micellar interface without an increase of the shell SLD. This could appear in contradiction except if we consider a partial dehydration when nitrate ions are adsorbed onto the micellar surface.

Competition between Chloride and Nitrate. In order to determine the preference of the CP interface for chloride or nitrate condensation or adsorption, two solutions of constant surfactant concentrations (10 mM) of CPC and CPN, respectively, in their corresponding acids are mixed. This was done at 0.1 and 1 M bulk acid concentrations, and the aggregation behavior as a function of the nitrate/chloride ratio was followed by light scattering. The result is shown in Figure 4.

The behavior versus mole fraction of chloride in counterions is far from ideal, nor follows regular solution theory. We are here in

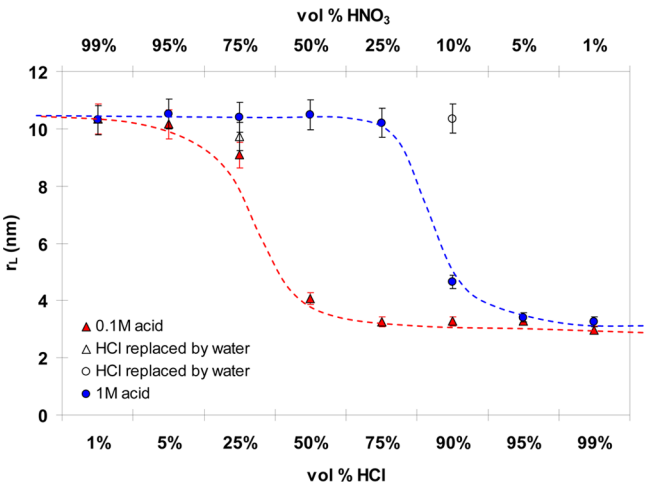

Figure 4. Apparent averaged hydrodynamic radius of cetylpyridinium aggregates at constant surfactant concentration (10 mM) in a mixture of nitric and hydrochloric acid at different ratios. Total acid concentrations are 0.1 M (red ▲) and 1 M (blue ●). The empty circle is the reference point without chloride for the blue series: 10 mM CP, 0.1 M HNO_3, HCl replaced by water. The empty triangle is the reference point without chloride for the red series: 10 mM CP, 0.075 M HNO_3, HCl is replaced by water.

the case of nonlinear competition of ions for the *same* interface. A similar situation has been described in detail by Petrache and Aroti in the case of zwitterionic lipids.[43,44]

In Figure 4, we can see, also in the case of cationic surfactants, the competition between chloride and nitrate when comparing the point at 25 vol % HCl/75 vol % HNO_3 with the blank sample without chloride. The threshold concentration of bulk nitrate necessary to induce a sphere-to-rod transition of 10 mM CPN micelles is between 25 and 50 mM. Moreover, not only the ratio of chloride and nitrate but also the total counterion concentration and the excess of counterions in solution influence aggregation. The preferential adsorption of nitrate on the micellar interface compared to chloride is in line with the analysis from the scattering spectra. This can be explained by favored interactions of chaotropes with chaotropes, as the pyridinium head group and nitrate belong to this category. It is nevertheless interesting to see that the presence of chloride has an influence on this preferential adsorption.

Lateral Equation of State (EOS). The structural data on cetylpyridinium aggregates obtained in the previous parts of this work can be used to determine the influence of anions on the free energy of the polar head group in an aggregate, resulting in an equation of state (EOS). "Lateral" EOS has been introduced in the field of lipids by S. Marcelja and J. Ennis.[45] In determining the surface per polar head when the derivative of free energy versus area is zero, this equation allows to quantify the different interactions between the surfactant heads within the aggregates whatever their shape, globular, cylindrical, or planar (monolayer or bilayer). Few articles focus on the determination of the lateral equation of state,[46,47] and there is no generally established method to separate all energetic contributions to the EOS. Up to now in most studies, osmotic stress experiments were carried out on phospholipid bilayers or catanionic vesicles as model systems[46−50] to vary through the water activity the hydration of the polar heads. In contrast to former works, where globally neutral lipid−water interfaces were considered, the reference state here consists in this work of small spherical micelles with a highly curved and charged interface. It has to be noted that we treat only spherical micelles in this approach.

We focus on three main contributions to the total free energy: (i) the hydrocarbon−water free energy which is modeled with a term of the interfacial tension, (ii) the short-range steric repulsion energy of the surfactant head groups, and (iii) the electrostatic energy of interaction between the charged pyridinium head groups and the "associated" or "associated and adsorbed" counterions onto the micelle, respectively. This last point requires a self-consistent definition of association and adsorption. Like Aswal and co-workers,[40] we consider the chloride counterion as associated but not adsorbed, as we found that no sphere-to-rod transition of 10 mM CPC occurs in 3 M HCl solutions. In this context, Collins proposed a difference in matching water affinities to explain this difference in counterion binding.[15] Here, we assume therefore that chloride does not penetrate the head group layer of the micelle but stays in close vicinity of the polar head: we will talk about a weak binding or *counterion association*. In contrast, we have observed that the nitrate counterion can induce a sphere-to-rod transition for the micelles, meaning a stronger bond with the pyridinium heads qualified as an ion *adsorption*. We are aware that this is a rather simple way to distinguish between chloride and nitrate. Recently, Moreira et al.[51] presented a model that accounts for ionic specificity due to cosphere overlap between head group and counterions with several terms. In our model, we will account

dx.doi.org/10.1021/jp3093622 | J. Phys. Chem. B 2013, 117, 1345−1356

only for the mixing entropy due to adsorption of ions as well as the finite size of the adsorbed ions. The solubility decrease of hydrocarbons in electrolyte solutions and the effect of added salt on the interfacial tension as well as the dielectric constant and the density of the electrolyte solution are not included in our model.

The relation between the adsorption of nitrate ions and the geometry of the micelles can be understood thanks to a simple model. Both considerations are summarized in Figure 5 with

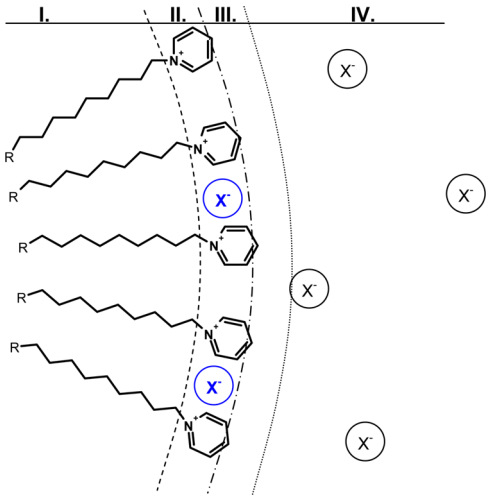

Figure 5. Schematic view of a partial cetylpyridinium micelle with its counterion distribution. The micelle is divided voluntarily into four different zones: (**I**) the hydrocarbon core where no counterions are supposed to be located; (**II**) the head group region, alias Stern layer, where a counterion can be found when it is adsorbed (the thickness of this layer is modeled with 3.6 Å, the length of one pyridinium ring); (**III**) the Palisade layer including water "bound by more than 1 kT to head groups"; (**IV**) the outside part of the diffuse layer where the counterions are supposed to be "free", since they are bound by less than 1 kT to the surfactant and subject to Poisson−Boltzmann type of equilibrium.

either an adsorption of the anion on the polar head (the nitrate case) or a classical screening within a Debye layer around the micelle. The three main contributions presented above account for the total free energy of the polar corona, which can be written as a function of the surface area per head group a:

$$F_{\text{total}} = F_{\text{L/W}} + F_{\text{head-rep}} + F_{\text{el}} \quad (10)$$

Each term is detailed in the Appendix. The first term $F_{\text{L/W}}$ corresponds to the lateral equation of state that comes from the short-range attractive forces. The second one $F_{\text{head-rep}}$ stands for the repulsion between the head groups. The last one F_{el} represents the electrostatic interactions. This ionic term depends on the ionic atmosphere around the micelle. In the case of adsorption (nitrate ion), this term is calculated by taking into account the chemical equilibrium between the adsorbed (intercalated) ions and the free ones.

The input parameters are N_{agg}, the aggregation number, R_{coll}, the radius of the micelle, the ionic strength, and finally a_{max}. In order to give a more descriptive idea of the output, we plotted the free energy of the polar head group (eq 10) as a function of the surface area a for the sample of 10 mM CPC in 0.01 M HCl in the graph in Figure 6 (top). The same procedure was applied for the sample 10 mM CPN in 0.01 M HNO_3 and is shown in Figure 6 (bottom). From the graphs, we can then extract the equilibrium surface area, a_{EOS}, that is clearly different for both cases presented above.

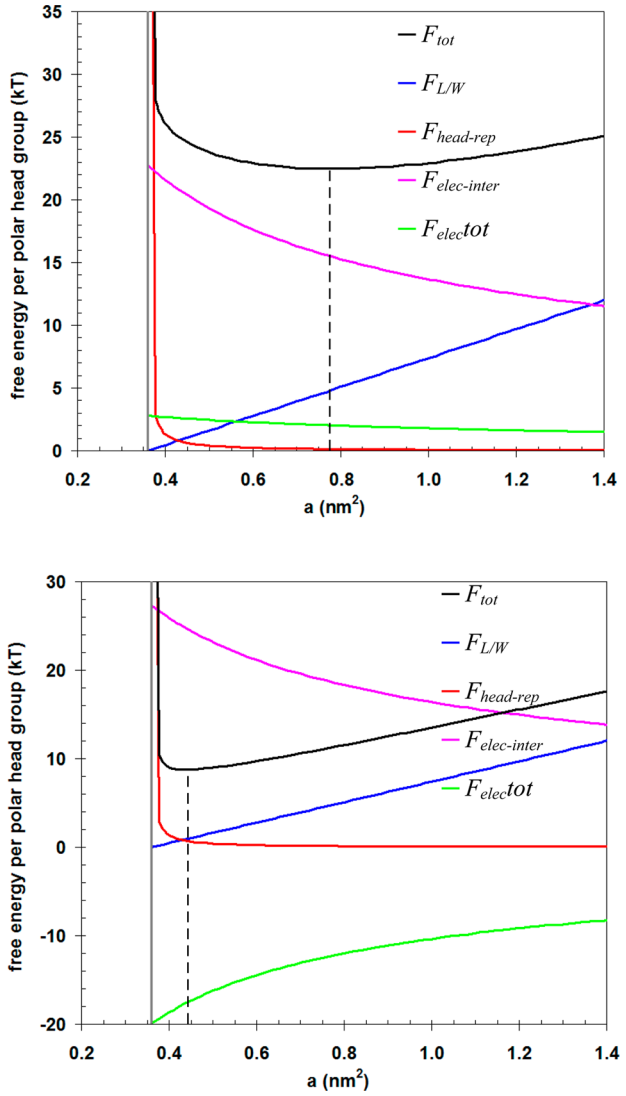

Figure 6. Energetic contributions to the total free energy F_{tot} per polar head group (in k_BT units) for (upper graph) 10 mM CPC in 0.01 M HCl and (lower graph) 10 mM CPN in 0.01 M HNO_3. $F_{\text{L/W}}$ means the energy needed to create the hydrocarbon−water interface. $F_{\text{head-rep}}$ and $F_{\text{elec-inter}}$ account for the steric and short-range repulsion between the surfactant head groups, respectively. F_{elec}tot is the electrostatic energy coming from the association and adsorption of nitrate close to the surfactant head groups. The vertical gray line stands for the minimal steric surface area (0.36 nm^2) and the black dashed line for the equilibrium surface area a_{EOS} of 0.77 and 0.44 nm^2 for CPC and CPN head groups, respectively.

We can see in Figures 5 and 6 that the major contributions in the electrostatic term (see figure in the Appendix) come from the "packing term" which is due to the loss of entropy of the intercalated ions and from the electrostatic term. The other terms contribute only as minor corrections. For the case of the pure "associated" ions like chloride, the packing term is described by a vertical line as a function of N_{ads} and only the ordinate value of the F_{PB} term is taken into consideration and varies as a function of a.

Concerning the a_{EOS} values at equilibrium, the minimum of F_{tot} is located at 0.77 nm^2 for CPC/0.01 M DCl and at 0.44 nm^2 for CPN/0.01 M DNO_3. A comparison of calculated a_{N} and a_{EOS} for spherical CPC and CPN micelles, respectively, in solutions at different ionic strength is given in Table 4.

dx.doi.org/10.1021/jp3093622 | J. Phys. Chem. B 2013, 117, 1345−1356

Table 4. Comparison of the Surface Area per Head Groups a_N (nm^2) Determined by SANS with Their Counterparts a_{EOS} (nm^2) Obtained by the Free Energy Model

chloride system	water	0.01 M chloride	0.1 M chloride
a_N	0.6	0.6	0.6
a_{EOS}	0.72	0.77	0.81
nitrate system	water	0.01 M nitrate	0.1 M nitrate
a_N	0.56	0.56	
a_{EOS}	0.44	0.44	

We can see that a_{EOS} slightly increases with increasing ionic strength for the chloride case, while the experimental values from the SANS remain constant (we can just point out that from SAXS data we can observe an increase of the surface per polar head only at high ionic strength, up to 1 M in DCl). The absolute difference between the two data sets is rather low but visible and becomes maximal for the data set at 0.1 M HCl. Nevertheless, we can say that the different contributions which influence a are satisfyingly taken into account within the model. In the case of nitrate, the calculated a_{EOS} remains constant at 0.44 nm^2, which is close to the purely steric head group area of 0.36 nm^2. The reason for this small value comes from the important contribution of the electrical term due to nitrate adsorption. The absolute value, though, is smaller than the one measured by SANS at 0.56 nm^2. Nevertheless, the model succeeds in discriminating between the two types of counterions and provides reasonable absolute surface per head group areas. The introduction of a background salt does not change appreciably the value of a_{EOS}. It is more interesting to see the change when chloride is replaced by nitrate as the counterion; in this case, a_{EOS} is reduced significantly. At higher ionic strengths, no further change of a_{EOS} is observed for chloride. The limit of the Poisson−Boltzmann approach is reached, as the activity of the ions which becomes important in these conditions is not taken into account.

CONCLUSION

In this study, we have shown the influence of two "classical" counterions chloride and nitrate as well as the more special counterions oxalate on the aggregation behavior of the cationic surfactant cetylpyridinium in the corresponding acid solution.

We have shown the influence of the type of counterion on micellization parameters (cmc, T_K) as well as structural parameters of the aggregates (r, N_{Agg}, a). T_K is found to be much higher for CP_2Ox than for CPC and CPN, while the inverse tendency was observed and measured for the cmc; the latter increases in the series CP_2Ox < CPN < CPC. These rather surprising results indicate that CP_2Ox behaves more like a double-chain surfactant than a single-chain surfactant. We explain this by the fact that oxalate counterions bridge two cetylpyridinium head groups but without influencing too much the curvature of the aggregates. Despite the differences between the three surfactants, at first approximation, spherical aggregates are the preferred aggregation form for the three surfactants at low ionic strength (<0.01 M), but at higher ionic strength (>0.01 M), CPN undergoes a sphere-to-rod transition, while CPC and CP_2Ox aggregates remain spherical. This proves that different interactions between the aggregates and the counterions take place. The results for nitrate are explained by an adsorption of the chaotropic nitrate within the micellar interface, while the kosmotropic chloride interacts less strongly with the micelle. These results go hand in hand with the position of the anion within the Hofmeister series. Oxalate can be regarded as a kosmotrope, too, as we find a spherical geometry of the CP_2Ox aggregates; this clearly proves that there is no adsorption of oxalate at the micellar interface and that the interactions are purely of electrostatic nature.

Moreover, the results for CPC and CPN could be described by a free energy model, which successfully discriminates between the interaction of chloride and nitrate concerning the micellar surface. The equilibrium head group surface area of CPC was determined with 0.72 nm^2, which is about 15% higher than the value determined by SANS, while the head group area for CPN due to nitrate adsorption (0.44 nm^2) is smaller than the experimentally determined value at 0.56 nm^2.

APPENDIX

Three main contributions are taken into account for the total free energy (F_{total}) of the polar corona. They are written as a function of the surface area per head group a:

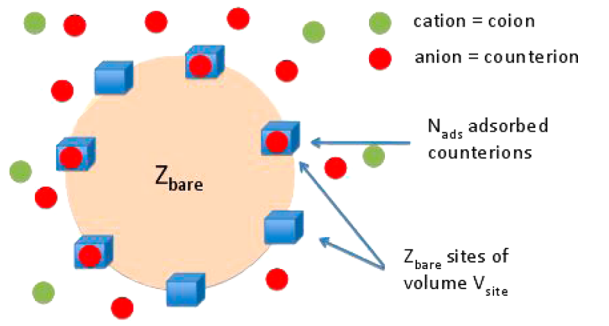

Figure 7. Model of the micelles. N_{ads} anions are absorbed in Z_{bare} sites located at the surface. Further around the colloid represents the Debye layer. The only driving force of the model corresponds to the electrostatic force (calculated at the Poisson−Boltzmann level of approximation), together with the entropic contribution. For chloride ions, V_{site} = 0 and there is no adsorption.

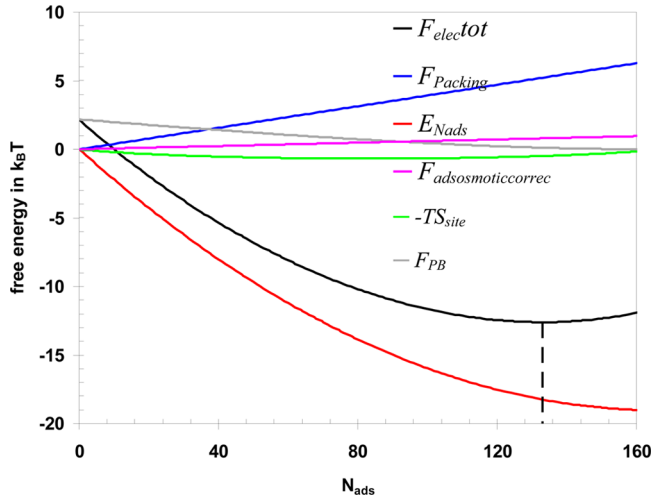

Figure 8. Energetic contributions to the total free energy F_{elec}tot per colloid (k_BT) for 10 mM CPN in 0.01 M HNO_3. $E_{N_{ads}}$ is the adsorption of the ions on the micellar surface, $-TS_{site}$ is the entropy of mixing, $F_{packing}$ is the packing entropy, $F_{ads\_osmoticcorrec}$ is the decrease in osmotic pressure due to nitrate adsorption (depletion of the bulk), and F_{PB} is the Poisson−Boltzmann free energy of the not adsorbed (free) ions. The dashed line marks the maximum of N_{ads} (133).

dx.doi.org/10.1021/jp3093622 | J. Phys. Chem. B 2013, 117, 1345−1356

$$F_{total} = F_{L/W} + F_{head\text{-}rep} + F_{el} \quad \text{(A-1)}$$

In this lateral equation of state (EOS), the surface tension term $F_{L/W}$ accounts for the constraint of creating an amphiphile−water interface and it is defined as

$$F_{L/W} = \gamma(a - a_0) \quad \text{(A-2)}$$

where γ denotes the surface tension of the amphiphile−water interface, a the head group area, and a_0 the minimal head group area arising from pure steric considerations and fixed at 0.36 nm^2. As γ is not directly accessible, the value of the pure hexadecane/water interface (47.5 $mN{\cdot}m^{-1}$) is taken as an approximation.[28] The second term in the EOS corresponds to the short-range repulsion between the head groups and can be expressed as[47]

$$F_{head\text{-}rep} = \frac{C_{\mu_{H_2O}}}{a - a_0} \quad \text{(A-3)}$$

This term diverges when two polar heads are in contact, and then. a simple power law in $(a - a_0)^{-1}$ is considered. The factor C depends only on the chemical potential of water. This parameter is adjusted for chloride and nitrate in our model, by considering that at zero bulk ionic strength the ion clouds around the micelle are homogeneous (and characterized by a large Debye length). Due to the Gauss theorem, the field inside these ion clouds is zero[52] and F_{el} is considered to be constant and negligible. Then, we can write for these conditions:

$$F_{total} = F_{L/W} + F_{head\text{-}rep} = 0 \quad \text{(A-4)}$$

The parameter C is deduced from this equation by taking a_G as the equilibrium value measured from tensiometry measurements at the CMC (taken for both systems chloride and nitrate a_G = 0.43 nm^2 [29]). It follows

$$C = \gamma(a - a_0)^2 \quad \text{(A-5)}$$

With γ = 47.5 $mN{\cdot}m^{-1}$ = 0.1154 $k_BT{\cdot}Å^{-2}$, we obtain C = 5.65 k_BT.

In the following part, the electrostatic energy term F_{el} is calculated thanks to a simple density functional theory at the local density approximation (DFT/LDA) for the ionic distributions, which corresponds to the Poisson−Boltzmann, equation for the ion profiles. Two different approaches can be proposed, depending on the possibility of adsorbing (intercalating) ions between the head groups at the surface. The global picture of the model solved in that appendix is represented in Figure 7. By doing so, we can distinguish between an "association" and an "association + adsorption". For kosmotropic counterions like chloride, a mean-field Poisson−Boltzmann approach is considered as sufficient to account for the electrostatic interactions. Indeed, we consider only the association of chloride with the pyridinium head groups in the Debye layer which can be modeled by the Poisson−Boltzmann equation. For nitrate, however, association and adsorption are both considered to take place. Nitrate can be intercalated between the head group. The general expression of the electrical term is given in eq A-6.

$$F_{elec}tot = \underbrace{\{E_{Nads} - TS_{site} - F_{packing}\}}_{\text{contribution 1 (adsorption)}} + \underbrace{\{F_{ads\_osmoticcorr} - F_{PB}\}}_{\text{contribution 2 (Debye layer)}} + \underbrace{F_{elec-inter}}_{\text{contribution 3 (polar head)}} \quad \text{(A-6)}$$

For a better understanding, this equation can be separated into three major contributions:

(1) The first contribution comes from the adsorption of ions on the micellar surface. In the model, the ions are N_{ads} simple ideal solutes intercalated between the polar heads. The adsorption phenomenon is represented by Z_{bare} adsorption sites of volume V_{site}. Each site may be filled by one ion. There is no specific energy but the electrostatic force. Straightforward calculations in the canonical ensemble show that the corresponding free energy is the sum of three terms $E_{N_{ads}}$, $-TS_{site}$, and $-F_{packing}$. Here, $E_{N_{ads}}$ stands for the electrostatic energy of the ions adsorbed to the surface and is given as

$$E_{N_{ads}} = \frac{e^2}{8\pi\varepsilon_0\varepsilon_1 R_{coll}}[Z_{bare} - N_{ads}]^2 \quad \text{(A-7)}$$

where e is the elementary charge, ε_0 and ε_r the dielectric constants of the vacuum and the solvent, respectively, R_{coll} is the radius of the colloid, Z_{bare} is the bare charge of the micelle (i.e., the aggregation number N_{Agg}), and N_{ads} is the number of adsorbed counterions. The second term is the contribution to the mixing entropy for adsorbed ions and defined as

$$-TS_{site} = -kT \ln C_{Z_{bare}}^{N_{ads}} \quad \text{(A-8)}$$

with $C_{Z_{bare}}^{N_{Ads}}$ being the binomial coefficient, i.e., the combination of adsorption sites and expressed as the factorial ratio $N_{ads}!/(N_{ads} - Z_{bare})!Z_{bare}!$ of the number of adsorbed ions N_{ads} and the number of available sites Z_{bare}.

The last term of this first contribution is the packing entropy, i.e., the loss of entropy due to the confinement of the adsorption of ions in sites of volume V_{site} between the polar heads. The terms read

$$\begin{aligned} F_{Packing} &= kTN_{ads} \ln(1/V_{site}) - kTN_{ads} \ln(\rho^0) \\ &= -kT{\cdot}N_{ads} \ln(\rho^0 V_{site}) \end{aligned} \quad \text{(A-9)}$$

This term is calculated with respect to the bulk phases in equilibrium with the adsorbed ions. ρ^0 is the volume fraction of the ions in this bulk phase.

(2) The second major contribution comes from the Debye layer of the ions around the colloid. In the LDA, the free energy of the ionic atmosphere is a functional of the cation density $\rho_+(\mathbf{r})$ and anion density $\rho_-(\mathbf{r})$.

$$\begin{aligned} F[\rho_+(\mathbf{r}), \rho_-(\mathbf{r})] = kT \sum_{i=+,-} \int d\mathbf{r}\rho_i(\ln(\rho_i\Lambda_i^3) - 1) \\ + \frac{1}{2}\int d\mathbf{r}\rho_{el}\phi \end{aligned} \quad \text{(A-10)}$$

where $\rho_{el} = (Z_+\rho_+ + Z_-\rho_-)e$ and ϕ is the (local) electrostatic potential (which depends on $\rho_+(\mathbf{r})$ and $\rho_-(\mathbf{r})$). Λ_i is the de Broglie length. Considering that the ions are equilibrated with a reservoir for which the electrostatic potential is zero and the concentrations ρ_i^0 and minimizing the density functional yields the following equilibrium profiles

$$\ln(\rho_i(\mathbf{r})\Lambda_i^3) + \frac{Z_i e}{kT}\phi(\mathbf{r}) = \ln(\rho_i^0\Lambda_i^3) \quad \text{(A-11)}$$

so that the free energy of the ionic atmosphere is

$$F_{DL} = kT \sum_{i=+,-} N_i[\ln(\rho_i^0\Lambda_i^3) - 1] - \frac{1}{2}\int d\mathbf{r}\rho_{el}\phi \quad \text{(A-12)}$$

When removing the constant terms that do not depend on the number of adsorbed ions N_{ads}, we get the following expression of the Debye layer free energy:

dx.doi.org/10.1021/jp3093622 | J. Phys. Chem. B 2013, 117, 1345−1356

$$F_2 = F_{ads\_osmoticcorr} - F_{PB} \quad \text{(A-13)}$$

Here, the first term stands for the decrease of osmotic pressure when a certain number of ions adsorb and is described as

$$F_{ads\_osmoticcorr} = kT \cdot N_{ads} \quad \text{(A-14)}$$

The positive sign comes from the fact that the free energy is calculated from the reference state for which there is no adsorption.

Finally, the last term is the electrostatic term that takes into account the electrostatic energy of the nonadsorbed ions, which are not distributed homogeneously around the micelle. It reads

$$F_{PB} = -\oint \rho_{el} V/2 \, d\vec{r} \quad \text{(A-15)}$$

The calculation of this term requires a numerical solution of the Poisson−Boltzmann equation for a spherical geometry obtained by a finite difference method in order to get $\rho_{el}(\mathbf{r})$ and $\phi(\mathbf{r})$.

(3) The third and last major contribution comes from the electrostatic repulsion between the polar heads when the radius of the micelle is changing. We can write this term for the charged micellar shell:

$$E = \frac{1}{2} \cdot \frac{Z_{bare}{}^2 e^2}{4\pi\varepsilon_0\varepsilon_1 \cdot R_{coll}} = \frac{Z_{bare}{}^2 \cdot L_B \cdot kT}{2R_{coll}} \quad \text{(A-16)}$$

where L_B is the Bjerrum length. Thus, the energy per surfactant molecule becomes

$$F_{elec\_inter} = \frac{Z_{bare} \cdot L_B}{2R_{coll}} \quad \text{(A-17)}$$

These considerations lead us to the definition of the following variables: a, R_{coll}, Z_{bare}, V_{site}, and N_{ads}. In order to simplify the approach, we can link R_{coll} with a, the polar head group area, by

$$R_{coll} = \sqrt{\frac{N_{Agg} \cdot a}{4\pi}} \quad \text{(A-18)}$$

Thus, when varying the surface per head group, the radius of the colloid will be affected, too. Z_{bare} is identical with N_{Agg} as described above. Furthermore, we define the volume of the adsorption site per head group (V_{site}) by calculating the total volume of the micellar shell (where the polar CP heads are located) and subtracting the constant volume that is sterically occupied by the CP heads. In this approach, each CP head group is considered to have a volume corresponding to $a_0 \cdot l$, where l is the length of a CP head group. For l, we take a value of 3.6 Å, determined by the software *Avogadro* for the length of one pyridinium ion, which lies in between the data published by Stigter (2.8 Å) and Heindl (6.0 Å). The total volume of all sites per micelle is

$$V_{site}^{tot} = [R_{coll}{}^3 - (R_{coll} - l)^3] \cdot \left(\frac{4}{3}\pi - \frac{a_0}{3R_{coll}{}^2}\right) \quad \text{(A-19)}$$

and V_{site} results by

$$V_{site} = \frac{V_{site}^{tot}}{N_{Agg}} \quad \text{(A-20)}$$

Our approach now consists of minimizing equation A-6 first with respect to a_{min} and N_{ads}. The minimization with respect to N_{ads} corresponds to the chemical equilibrium between the adsorbed and free counterions. The minimization with respect to a_{min} gives the equilibrium size of the micelle.

It has to be noted that for a kosmotropic counterion like chloride, which does not adsorb according to our model, V_{site} equals zero and the three middle terms of eq II.12 are left out. Only the contribution of the electrostatic energy of adsorption $E_{N_{ads}} = (e^2/8\pi\varepsilon_0\varepsilon_1 R_{coll})[Z_{bare}]^2$ and the free energy calculated by the Poisson−Boltzmann approach $F_{PB} = -{}^1/_2 \int d\mathbf{r} \rho_{el} \phi$ remain. In contrast, for a chaotropic counterion like nitrate, we consider a partial adsorption in the sites of the micellar interface and all six contributions of eq A-6 influence the calculation of the electric energy.

In the general part, we plotted the free energy of the polar head group (eq A-1) as a function of the surface area a for the sample of 10 mM CPC/0.01 M HCl and the sample 10 mM CPN/0.01 M HNO_3 in the graphs in Figure 6.

In this appendix, we can just plot the different contribution of F_{elec}tot as a function of N_{ads} for a given a, and in Figure 8, we have chosen $a = a_{EOS}$.

■ ASSOCIATED CONTENT

Supporting Information

Infrared spectra and elementary analysis of CPC, CPN, and CPOx; surface tension isotherms; speciation of oxalic acid; dynamic and static light scattering; SANS experiments; and SAXS experiments. This material is available free of charge via the Internet at http://pubs.acs.org.

■ AUTHOR INFORMATION

Corresponding Author

*Mailing address: CEA Marcoule, ICSM Bat. 426, BP 17171, 30207 Bagnols-sur-Cèze cedex, France. Phone: +33 (0) 466339209. Fax: +33 (0)466797611. E-mail: olivier.diat@cea.fr.

Present Address

†Laboratoire des Interactions Moléculaires et Réactivité Chimique et Photochimique (IMRCP), UMR 5623 (CNRS/Université Paul Sabatier), Toulouse, France.

Notes

The authors declare no competing financial interest.

■ ACKNOWLEDGMENTS

The authors thank the ESRF for providing beamtime for SAXS experiments (SC2636) and more especially Cyril Rochas for his help as a local contact. Part of this research is founded by GNR PARIS from PACEN. LLB provides us also some important research time necessary for our studies with the help of J. Jestin as local contact and M. Detrez for his technical assistance.

■ REFERENCES

(1) Atia, A. A.; Saleh, M. M. *J. Appl. Electrochem.* **2003**, *33*, 171−177.
(2) Jenkins, S.; Addy, M.; Wade, W.; Newcombe, R. G. *J. Clin. Periodontol.* **1994**, *21*, 397−401.
(3) Pandey, S.; Acree, W. E.; Fetzer, J. C. *Talanta* **1998**, *47*, 769−778.
(4) Baek, K.; Yang, J. W. *Desalination* **2004**, *167*, 101−110.
(5) Alizadeh, N.; Salimi, S.; Jabbari, A. *Sep. Purif. Technol.* **2002**, *28*, 173−180.
(6) Chevalier, Y.; Zemb, T. *Rep. Prog. Phys.* **1990**, *53*, 279−371.
(7) Kunz, W. *Specific ion effects*, 1st ed.; World Scientific Publishing Company: 2009.
(8) Kunz, W.; Henle, J.; Ninham, B. W. *Curr. Opin. Colloid Interface Sci.* **2004**, *9*, 19−37.
(9) Pinna, M. C.; Bauduin, P.; Touraud, D.; Monduzzi, M.; Ninham, B. W.; Kunz, W. *J. Phys. Chem. B* **2005**, *109*, 16511−16514.
(10) Zhang, Y. J.; Cremer, P. S. *Curr. Opin. Chem. Biol.* **2006**, *10*, 658−663.

(11) Leontidis, E. *Curr. Opin. Colloid Interface Sci.* **2002**, *7*, 81−91.
(12) Lo Nostro, P.; Lo Nostro, A.; Ninham, B. W.; Pesavento, G.; Fratoni, L.; Baglioni, P. *Curr. Opin. Colloid Interface Sci.* **2004**, *9*, 97−101.
(13) Schwierz, N.; Horinek, D.; Netz, R. R. *Langmuir* **2010**, *26*, 7370−7379.
(14) Vlachy, N.; Jagoda-Cwiklik, B.; Vacha, R.; Touraud, D.; Jungwirth, P.; Kunz, W. *Adv. Colloid Interface Sci.* **2009**, *146*, 42−47.
(15) Collins, K. D. *Biophys. J.* **1997**, *72*, 65−76.
(16) Bostrom, M.; Williams, D. R. M.; Ninham, B. W. *Langmuir* **2002**, *18*, 6010−6014.
(17) Geng, Y.; Romsted, L. S.; Froehner, S.; Zanette, D.; Magid, L. J.; Cuccovia, I. M.; Chaimovich, H. *Langmuir* **2005**, *21*, 562−568.
(18) Romsted, L. S. *Langmuir* **2007**, *23*, 414−424.
(19) Vlachy, N.; Drechsler, M.; Verbavatz, J. M.; Touraud, D.; Kunz, W. *J. Colloid Interface Sci.* **2008**, *319*, 542−548.
(20) Abezgauz, L.; Kuperkar, K.; Hassan, P. A.; Ramon, O.; Bahadur, P.; Danino, D. *J. Colloid Interface Sci.* **2010**, *342*, 83−92.
(21) Aswal, V. K.; Goyal, P. S.; Menon, S. V. G.; Dasannacharya, B. A. *Physica B* **1995**, *213*, 607−609.
(22) Kumar, S.; Bansal, D.; Kabir-ud-Din. *Langmuir* **1999**, *15*, 4960−4965.
(23) Anacker, E. W. *J. Phys. Chem.* **1958**, *62*, 41−45.
(24) Anacker, E. W.; Ghose, H. M. *J. Am. Chem. Soc.* **1968**, *90*, 3161−3166.
(25) Bhat, M. A.; Dar, A. A.; Amin, A.; Rashid, P. I.; Rather, G. M. *J. Chem. Thermodyn.* **2007**, *39*, 1500−1507.
(26) Heckmann, K.; Schwarz, R.; Strnad, J. *J. Colloid Interface Sci.* **1987**, *120*, 114−117.
(27) Perche, T.; Auvray, X.; Petipas, C.; Anthore, R.; Perez, E.; RicoLattes, I.; Lattes, A. *Langmuir* **1996**, *12*, 863−871.
(28) Semmler, A.; Kohler, H. H. *J. Colloid Interface Sci.* **1999**, *218*, 137−144.
(29) Varade, D.; Joshi, T.; Aswal, V. K.; Goyal, P. S.; Hassan, P. A.; Bahadur, P. *Colloids Surf., A* **2005**, *259*, 95−101.
(30) Evans, D. F.; Mitchell, D. J.; Ninham, B. W. *J. Phys. Chem.* **1984**, *88*, 6344−6348.
(31) Sasaki, S. *J. Phys. Chem. B* **2007**, *111*, 2473−2476.
(32) Sasaki, S. *J. Phys. Chem. B* **2009**, *113*, 8545−8551.
(33) Nakayama, H.; Shinoda, K. *Bull. Chem. Soc. Jpn.* **1967**, *40*, 1797−1799.
(34) Debye, P. *J. Phys. Colloid Chem.* **1947**, *51*, 18−32.
(35) Hayter, J. B.; Penfold, J. *Colloid Polym. Sci.* **1983**, *261*, 1022−1030.
(36) Ezquerra, T. A.; Garcia-Gutierrez, M. C.; Nogales, A.; Gomez, M. *Applications of Synchrotron Light to Scattering and Diffraction in Materials and Life Sciences*; Springer: Berlin, 2009; Vol. *776*.
(37) Fedors, R. F. *Polym. Eng. Sci.* **1974**, *14*, 147−154.
(38) Odijk, T. *J. Phys. Chem.* **1989**, *93*, 3888−3889.
(39) Zemb, T.; Diat, O. *XIV International Conference on Small-Angle Scattering (Sas09)* 2010, *247*.
(40) Aswal, V. K.; Goyal, P. S.; Amenitsch, H.; Bernstorff, S. *Pramana* **2004**, *63*, 333−338.
(41) Heindl, A.; Kohler, H. H. *Langmuir* **1996**, *12*, 2464−2477.
(42) Stigter, D. *J. Phys. Chem.* **1974**, *78*, 2480−2485.
(43) Aroti, A.; Leontidis, E.; Dubois, M.; Zemb, T.; Brezesinski, G. *Colloids Surf., A* **2007**, *303*, 144−158.
(44) Petrache, H. I.; Belloni, L.; Zemb, T.; Parsegian, V. A. *Biophys. J.* **2005**, *88*, 236a−236a.
(45) Ennis, J. *J. Chem. Phys.* **1992**, *97*, 663−678.
(46) Leontidis, E.; Aroti, A.; Belloni, L.; Dubois, M.; Zemb, T. *Biophys. J.* **2007**, *93*, 1591−1607.
(47) Zemb, T.; Belloni, L.; Dubois, M.; Aroti, A.; Leontidis, E. *Curr. Opin. Colloid Interface Sci.* **2004**, *9*, 74−80.
(48) Fattal, D. R.; Andelman, D.; Benshaul, A. *Langmuir* **1995**, *11*, 1154−1161.
(49) Harries, D.; Podgornik, R.; Parsegian, V. A.; Mar-Or, E.; Andelman, D. *J. Chem. Phys.* **2006**, *124*, No. 224702.
(50) Yuet, P. K.; Blankschtein, D. *Langmuir* **1996**, *12*, 3802−3818.
(51) Moreira, L.; Firoozabadi, A. *Langmuir* **2010**, *26*, 15177−15191.
(52) Akoum, F.; Parodi, O. *J. Phys.* **1985**, *46*, 1675−1681.